

Osmolality-Dependent Relocation of Penicillin-Binding Protein PBP2 to the Division Site in *Caulobacter crescentus*

Jason Hocking,^a Richa Priyadarshini,^{b*} Constantin N. Takacs,^{b*} Teresa Costa,^{b*} Natalie A. Dye,^c Lucy Shapiro,^d Waldemar Vollmer,^e and Christine Jacobs-Wagner^{a,b,f}

Howard Hughes Medical Institute, Yale University, New Haven, Connecticut, USA^a; Department of Molecular, Cellular and Developmental Biology, Yale University, New Haven, Connecticut, USA^b; Howard Hughes Medical Institute and Department of Biochemistry, Stanford University School of Medicine, Stanford, California, USA^c; Department of Developmental Biology, Stanford University School of Medicine, Stanford, California, USA^d; Centre for Bacterial Cell Biology, Institute for Cell and Molecular Biosciences, Newcastle University, Newcastle upon Tyne, United Kingdom^e; and Section of Microbial Pathogenesis, Yale School of Medicine, New Haven, Connecticut, USA^f

The synthesis of the peptidoglycan cell wall is carefully regulated in time and space. In nature, this essential process occurs in cells that live in fluctuating environments. Here we show that the spatial distributions of specific cell wall proteins in *Caulobacter crescentus* are sensitive to small external osmotic upshifts. The penicillin-binding protein PBP2, which is commonly branded as an essential cell elongation-specific transpeptidase, switches its localization from a dispersed, patchy pattern to an accumulation at the FtsZ ring location in response to osmotic upshifts as low as 40 mosmol/kg. This osmolality-dependent relocation to the division apparatus is initiated within less than a minute, while restoration to the patchy localization pattern is dependent on cell growth and takes 1 to 2 generations. Cell wall morphogenetic protein RodA and penicillin-binding protein PBP1a also change their spatial distribution by accumulating at the division site in response to external osmotic upshifts. Consistent with its ecological distribution, *C. crescentus* displays a narrow range of osmotolerance, with an upper limit of 225 mosmol/kg in minimal medium. Collectively, our findings reveal an unsuspected level of environmental regulation of cell wall protein behavior that is likely linked to an ecological adaptation.

Most bacteria possess a peptidoglycan (PG) polymer as a major component of their cell wall. The PG consists of glycan chains that are linked covalently by short peptides, resulting in a strong, elastic meshwork that surrounds the cytoplasmic membrane (36). Under most conditions, this PG meshwork is essential for cell viability by providing a mechanical resistance to the turgor pressure caused by the high concentration of solutes in the cytoplasm relative to the environment. The PG layer also plays a structural role by maintaining cell shape. Growth of the PG requires the coordinated actions of both synthetic and lytic enzymes (22) and is regulated by the cytoskeleton (5) and, at least in some Gram-negative bacteria, by specific outer-membrane lipoproteins (24, 33). During cell elongation, most rod-shaped bacteria insert new PG material into the existing PG along the cylindrical sidewall following a patchy/helical pattern (9, 13). Division and new pole formation proceed by localized PG synthesis directed by the cyto-kinetic FtsZ ring and associated proteins. In some bacteria, such as *Caulobacter crescentus* (and possibly *Escherichia coli* to a lesser extent), a significant amount of cell elongation stems from FtsZ ring-dependent PG growth (1, 13, 34) in a process also known as preseptal growth (36).

Early studies in *E. coli* (29) suggest that the penicillin-binding proteins (PBPs) PBP2 and PBP3 are specifically involved in cell elongation and division, respectively. Both enzymes are inner-membrane proteins that catalyze the transpeptidation reaction linking adjacent glycan strands of the PG in the periplasm. Consistent with its role in division, PBP3 and homologs have been shown to localize at the FtsZ ring in various bacteria (7, 10, 37). Comparatively, the localization of PBP2 displays more variability among species. In *E. coli*, PBP2 is spatially distributed throughout the cell according to a reported patchy/helical pattern, with some ring-like accumulation in the midcell region (12, 35). In *C. cres-*

centus and *Helicobacter pylori*, PBP2 exhibits a patchy distribution throughout the cell with no midcell accumulations (14–16, 19). In contrast, in *Rhodobacter sphaeroides*, PBP2 is mostly concentrated in a midcell ring (28). It is unclear if such localization variability among species reflects differences in PBP2 activity, growth mode, experimental conditions, or adaptation to distinct habitats.

Besides PBP2, many other proteins are involved in cell wall morphogenesis (40). Some of these proteins are enzymes directly involved in peptidoglycan biosynthesis in either the cytoplasm (e.g., MurG) or the periplasm (such as PBPs) (40). Others (e.g., MreB, RodZ, RodA, MreC, and MreD) have important, albeit less well understood, cell shape functions (40). While cell wall morphogenetic proteins have been the focus of many studies, their behaviors have yet to be studied in situations of environmental flux, which occur in nature. In this study, we discovered that in *C. crescentus*, PBP2, RodA, and PBP1a change their spatial distribution in response to a small increase in external osmolality. Our

Received 21 February 2012 Accepted 5 April 2012

Published ahead of print 13 April 2012

Address correspondence to Christine Jacobs-Wagner, christine.jacobs-wagner@yale.edu.

* Present address: Richa Priyadarshini, Department of Molecular Genetics, The Forsyth Institute, Cambridge, Massachusetts, USA; Constantin N. Takacs, Laboratory of Cellular Biophysics, The Rockefeller University, New York, New York, USA; Teresa Costa, Instituto de Tecnologia Química e Biológica, Universidade Nova de Lisboa, Oeiras, Portugal.

Supplemental material for this article may be found at <http://jb.asm.org/>.

Copyright © 2012, American Society for Microbiology. All Rights Reserved.

doi:10.1128/JB.00260-12

TABLE 1 Strains and plasmids used in this study

Strain or plasmid	Genotype or description	Source
Strains		
<i>C. crescentus</i>		
CB15N	Also NA1000, synchronizable variant of the wild-type strain CB15	18
CJW1472	CB15N <i>xylX</i> ::pXGFP4C1	7
CJW1608	CB15N <i>murG</i> ::pBGentmurG-mgfp	1
CJW1715	CB15N <i>mreB</i> _{Q26P}	1
CJW2135	CB15N <i>xylX</i> ::pXGFP4-C1-PBP2	This work
CJW2742	CB15N <i>pbp2</i> :: <i>gfp</i> - <i>pbp2</i>	This work
CJW2908	CB15N <i>xylX</i> ::pXCFFN-1rodZ	3
CJW2951	CB15N <i>ftsZ</i> ::pVMCS-6ftsZ5'	3
CJW3207	CB15N <i>xylX</i> ::pXYFPN-2-rodA	This work
CJW3211	CB15N <i>xylX</i> ::pXCFFN-5-pbp2	This work
CJW3288	CB15N <i>xylX</i> ::pXGFPN5-pbp1a	This work
CJW3396	CB15N <i>xylX</i> ::pXCFFN-5-pbp2 <i>ftsZ</i> ::pVMCS-6ftsZ5'	This work
CJW3397	CB15N <i>xylX</i> ::pXGFP7-C1-YFP- <i>mreB</i> ::pXCFFN-5-pbp2	This work
CJW3402	CB15N <i>vanA</i> ::pMT400 <i>xylX</i> ::pXCFFN-5-pbp2	This work
CJW3403	CB15N <i>mreB</i> _{Q26P} <i>xylX</i> ::pXGFP4-C1-pbp2	This work
CJW4620	CB15N <i>xylX</i> ::pXGFPN5-pbp1a <i>vanA</i> ::pVCHYN1-pbp2	This work
CJW4621	CB15N <i>xylX</i> ::pXYFPN-2-rodA <i>vanA</i> ::pVCHYN1-pbp2	This work
JAT878	CB15N <i>vanA</i> ::pVCHYN1-pbp2	This work
LS4276	CB15N <i>xylX</i> ::pXGFP7-C1-yfp- <i>mreB</i>	15
LS4284	CB15N <i>xylX</i> :: <i>mreC</i> - <i>mcherry</i>	15
<i>E. coli</i>		
DH5 α	Cloning strain	Invitrogen
LMC1840	MC4100 <i>lysA</i> Δ (λ attL- <i>lom</i>):: <i>bla</i> <i>lacI</i> ^a pTB017- <i>gfp</i> - <i>pbp2</i>	11
S17-1	RP4-2; Tc::Mu; KM-Tn7, for plasmid mobilization	26
Plasmids		
pMT400	Integrative plasmid carrying <i>ftsZ</i> - <i>yfp</i> under vanillate-inducible expression	31
pVCHYN-1	Integrative plasmid for xylose-inducible expression of an mCherry fusion	31
pVCHYN1-pbp2	Integrative plasmid carrying <i>mcherry</i> - <i>pbp2</i> under vanillate-inducible expression	This work
pXGFP4C1	Integrative plasmid for xylose-inducible expression of GFP-PBP2	15
pXCFFN-5	Integrative plasmid for xylose-inducible expression of a CFP fusion	31
pXCFFN-5-pbp2	pXCFFN-5 carrying <i>gfp</i> - <i>pbp2</i> under xylose-inducible expression	This work
pXYFPN-5	Integrative plasmid for xylose-inducible expression of a YFP fusion	31
pXGFPN-5	Integrative plasmid for xylose-inducible expression of a GFP fusion	31
pXGFPN5-pbp1a	pXGFPN-5 carrying <i>gfp</i> - <i>pbp1a</i> under xylose-inducible expression	This work
pXYFPN-2-rodA	pXYFPN-2 carrying <i>rodA</i>	This work
pXGFP4-1MreB	Integrative vector carrying <i>gfp</i> - <i>mreB</i> under xylose-inducible expression	20
pXGFP4-C1-pbp2	Integrative vector carrying <i>gfp</i> - <i>pbp2</i> under xylose-inducible expression	This work
pNTPS138gfp-pbp2	Plasmid for integrating <i>gfp</i> - <i>pbp2</i> at its native locus in place of wild-type <i>pbp2</i>	This work

findings unravel a surprising environmental regulation that may reflect an ecological adaptation.

MATERIALS AND METHODS

Strains, plasmids, and growth conditions. The strains and plasmids used in this study are listed in Table 1, and the construction method is provided in the supplemental material. *C. crescentus* strains were grown in peptone yeast extract (PYE) medium (2 g/liter Bacto peptone, 1 g/liter yeast extract, 1 mM MgSO₄, and 0.5 mM CaCl₂) or defined minimal (M2G) medium (0.87 g/liter Na₂HPO₄, 0.54 g/liter KH₂PO₄, 0.50 g/liter NH₄Cl, 0.2% [wt/vol] glucose, 0.5 mM MgSO₄, 0.5 mM CaCl₂, and 0.01 mM FeSO₄) under aerobic conditions at 30°C (17) unless otherwise stated. Antibiotics were added when appropriate. Transformations, conjugation, and transductions were performed as previously described (17). Synchronization of cell populations with respect to the cell cycle was performed as previously described (18). Induction of gene expression from the xylose- or vanillate-inducible promoter was achieved by adding xylose or vanillic acid to the growth medium at the final concentrations of 0.03% and 0.5 mM, respectively,

except for the experiments shown in panels D of Fig. 1 and 2, for which 0.3% xylose was used. The presence of 0.03% xylose and 0.5 mM vanillic acid increases the osmolality of the solution by approximately 1.9 and 0.5 mosmol, respectively.

E. coli strains were grown in M9 glucose (M9G; 42 mM Na₂HPO₄, 22 mM KH₂PO₄, 8.5 mM NaCl, 1.9 mM NH₄Cl, 0.2% glucose, 1 mM MgSO₄, 3.3 μ M thiamine) or LB (10 g/liter tryptone, 5 g/liter yeast extract, and 10 g/liter NaCl) medium at 37°C with antibiotics when appropriate. Exponentially growing cultures were used in all experiments. Induction of gene expression from the IPTG (isopropyl- β -D-thiogalactopyranoside)-inducible promoter was achieved by adding IPTG to the growth medium at the final concentration of 100 μ M (adding ~0.1 mosmol to the solution).

Light microscopy. Imaging was performed using 100 \times differential interference contrast (DIC) or phase-contrast objectives on a Nikon E1000 microscope equipped with a Hamamatsu Orca-ER camera, on a Nikon Eclipse 80i microscope equipped with Andor iXon^{EM+} (DU-897E) EMCCD and Hamamatsu Orca II-ER cameras, or a Nikon Eclipse Ti-U microscope with a Hamamatsu Orca-ER camera. Cells were

mounted on 1% agarose pads made with the indicated medium. Images were taken with Metamorph software (Molecular Devices).

Image analysis. Cell identification and analysis were performed using the MATLAB-based, open-source software MicrobeTracker (27). “Demographs” were created by segmenting each cell, integrating the fluorescence in each segment, normalizing the fluorescence by the brightest segment of each cell, sorting cells by length, and plotting fluorescence values as a heat map from 0 (no fluorescence) to 1 (maximum-fluorescence segment in the cell). When appropriate, cells were oriented according to their pole identity prior to sorting. Cell polarity was determined either by using polar markers (for example, FtsZ-yellow fluorescent protein [YFP] accumulation identifies the new pole of swarmer cells) or by identifying the new pole generated during division in time-lapse recordings.

Osmolality measurements. Average osmolalities were calculated from three separate measurements using a Vapro Vapor Pressure 5520 osmometer (Wesco Biomedical Systems).

Growth rate measurements. To determine whether differences in growth rate cause midcell accumulation of PBP2, we first determined the doubling time of cultures growing at different temperatures. For this experiment, 25-ml flasks of culture were grown in a water bath shaker at the indicated temperature and growth medium. Samples were taken every hour for manual optical density reading at 660 nm (OD_{660}) using an Ultrospec 2100 Pro spectrophotometer. For the experiment shown in Fig. 6, cells were grown at 30°C in a Biotek Synergy2 96-well plate reader and optical density measurements (at 660 nm) were taken every 2 min. For each condition, a doubling time was determined by fitting an exponential curve to the interval represented by exponential growth. Averages and standard deviations (SDs) were obtained for three biological replicates for each condition.

Immunoblot analysis. For immunoblot analysis of cell extracts, cultures were grown under indicated conditions to an OD_{660} of 0.4 at 30°C. After growth, cells were harvested, resuspended in 100 μ l of 50 mM sodium phosphate buffer (pH 7.4) containing 50 mM NaCl and 1 mM EDTA, and sonicated. Whole-cell extracts were electrophoretically resolved on 12% SDS-PAGE gels, and the resolved proteins were electrotransferred to polyvinylidene difluoride (PVDF) membranes, which were probed with anti-green fluorescent protein (anti-GFP) antibodies (1:1,000; Clontech).

RESULTS

PBP2 accumulates at the FtsZ ring location. In *C. crescentus* cells, PBP2 has been reported to have a patchy/helical pattern of localization throughout the cell (14, 15, 19). Surprisingly, we found that when cells (strain JAT878) grown in rich PYE medium were imaged on an agarose pad containing M2G minimal medium (commonly used because M2G generates less fluorescence background than does the PYE medium), a vanillate-inducible, chromosomally expressed N-terminal mCherry fusion of PBP2 displayed a ring-like accumulation near midcell in many cells (Fig. 1A). We observed a similar localization pattern when using a GFP-PBP2 fusion expressed from either the xylose-inducible promoter (Fig. 1B) or the native *pbp2* promoter in place of wild-type *pbp2* (Fig. 1C), indicating that midcell localization occurs regardless of the type of fluorescent protein fused to PBP2 (GFP or mCherry) or the expression level of the fusion (inducible or native; see Fig. S1 in the supplemental material). Fusion to a fluorescent protein did not appear to affect the function of PBP2, since replacement of wild-type PBP2 by a GFP-PBP2 fusion (expressed from the native promoter on the chromosome in place of wild-type PBP2) supported viability and this strain did not display any apparent growth or morphological defects (data not shown).

We showed that the midcell localization was associated with specific cell cycle stages by examining the localization of both cyan fluo-

rescent protein (CFP)-PBP2 and FtsZ-YFP over time in synchronized cell cycle populations (strain CJW3402) grown in liquid PYE cultures (and spotted on an M2G agarose pad for visualization at 20-min intervals). At early cell cycle stages, GFP-PBP2 showed patchy localization throughout the cells with occasional accumulation at a cell pole (Fig. 1D). After FtsZ-YFP ring formation but before cell constriction became discernible, the intensity of the CFP-PBP2 signal throughout the cells diminished in favor of a ring-like (band) localization coinciding with the FtsZ-YFP ring near midcell (Fig. 1D). CFP-PBP2 remained colocalized with FtsZ-YFP throughout most of the cell constriction process (Fig. 1D).

PBP2 colocalizes with MreB at the FtsZ ring location in an FtsZ-dependent but MreB-independent manner. The FtsZ ring accumulation of PBP2 near midcell was surprising for at least two reasons. First, PBP2 is often referred to as a cell elongation-specific PBP, and second, the presence of MreB at the FtsZ ring has been proposed to prevent PBP2 from being recruited to that location (15). To examine the localization of PBP2 in large, unsynchronized cell populations, we imaged multiple fields of view and identified cells and their outline using the open-source image analysis software MicrobeTracker (27). The normalized fluorescence intensity was measured along the cell length, and then cells were sorted by cell length, to create what we call a demograph. Here, cell length was used as a measure of cell cycle progression. Figure 2A shows demographs of FtsZ-YFP and CFP-PBP2 localization in 1,000 cells producing both fluorescent fusions. The cell-length sorting reflects cell cycle progression, with smaller cells showing an accumulation of FtsZ-YFP at the new pole and longer cells displaying FtsZ-YFP accumulation near midcell (characteristic of the FtsZ ring). The corresponding demograph of CFP-PBP2 confirmed that PBP2 colocalizes with the FtsZ ring during a significant portion of the cell cycle. GFP-PBP2 was unable to form bands in FtsZ-depleted cells (Fig. 2B), indicating that recruitment of GFP-PBP2 near midcell is FtsZ dependent. We verified that GFP-PBP2 levels were unaffected under FtsZ-depletion conditions (see Fig. S2 in the supplemental material).

In *C. crescentus*, MreB localization has been reported to change during the cell cycle from a patchy pattern throughout the cell in the beginning of the cell cycle (stage 1) to an FtsZ ring-dependent midcell localization in the stalked and predivisional stages (stage 2) and back to a patchy pattern in the late predivisional stage (stage 3) (19, 20). Demographs of CJW3397 cells coproducing YFP-MreB and CFP-PBP2 confirm this previously noted three-stage cell cycle localization pattern for MreB (Fig. 2C). Interestingly, the patchy signal of YFP-MreB in the beginning of the cell cycle (stage 1) was most concentrated in the central region of the cells, as evident from the demograph (Fig. 2C). Similarly, in long, deeply constricted cells corresponding to the late predivisional stage (stage 3, Fig. 2C), the MreB-YFP patchy signal was most concentrated between the one-fourth and three-fourths regions, which correspond to the central regions of the future daughter cells. The biological significance of this pattern is unclear. However, more relevant to our PBP2 study, the corresponding demograph clearly shows that CFP-PBP2 colocalizes with MreB-YFP near midcell during stage 2 (Fig. 2C), indicating that MreB does not prevent PBP2 accumulation at the FtsZ ring under these conditions.

PBP2 localization at the FtsZ ring was independent of MreB. GFP-PBP2 bands near midcell were still discernible in cells treated with 50 μ M A22 (Fig. 2D), a drug that inhibits MreB polymeriza-

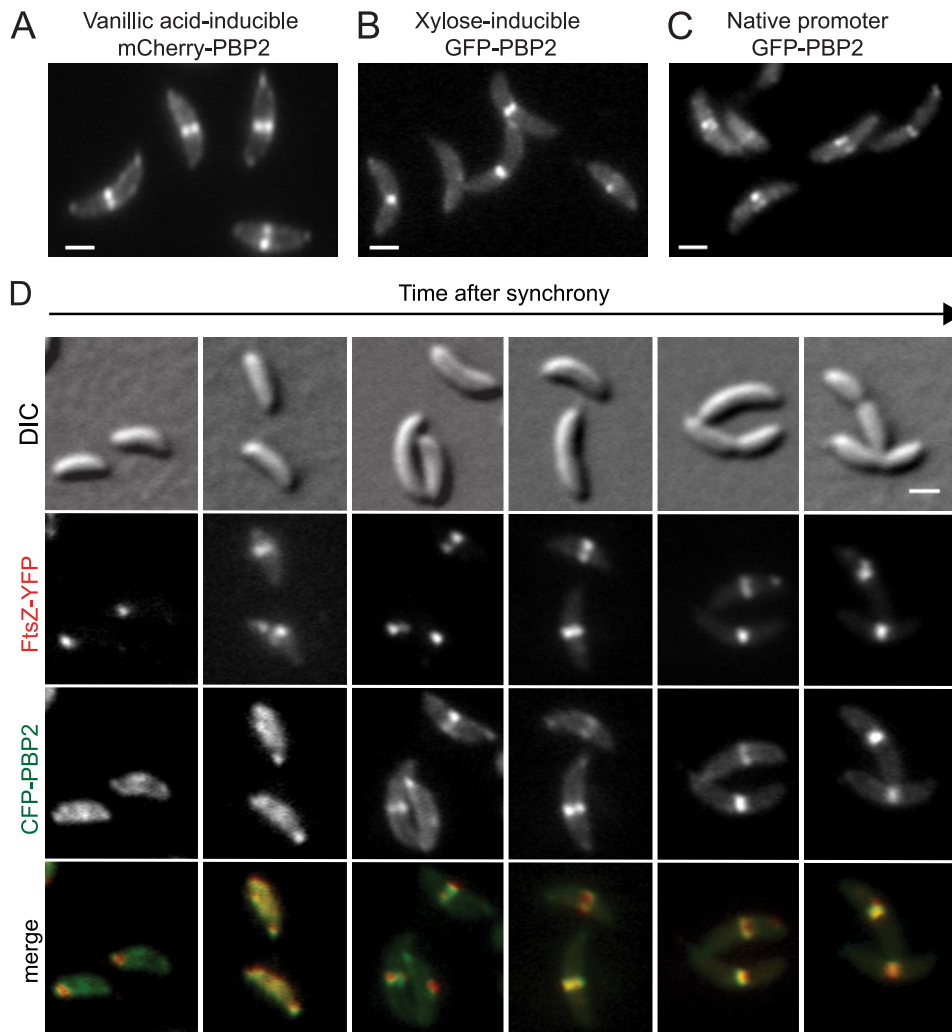


FIG 1 Accumulation of PBP2 at the FtsZ ring location. (A) JAT878 cells producing mCherry-PBP2 under the control of the vanillate-inducible promoter on the chromosome were grown in the presence of vanillic acid for 3 h in PYE medium before imaging on an M2G pad. (B) CJW2135 cells producing GFP-PBP2 under the control of the xylose-inducible promoter on the chromosome were grown in PYE with xylose for 3 h before imaging on an M2G pad. (C) CJW2742 cells producing GFP-PBP2 from the native promoter on the chromosome in place of wild-type PBP2 were grown in PYE and imaged on an M2G pad. Bar, 1 μm . (D) CJW3402 cells were grown in PYE with xylose for 2 h before synchronization. Synchronized swarmer cells were resuspended in PYE medium containing xylose, and samples were taken every 20 min for microscopy on M2G pads. Bar, 1 μm .

tion (4, 21). Since A22-treated cells have a cell shape defect and are rounder than untreated cells (21), we also examined GFP-PBP2 localization in *mreB*_{Q26P} mutant cells, which have a normal shape but produce an MreB mutant, MreB_{Q26P}, that largely fails to condense into a ring near midcell (1). Since GFP-PBP2 also retained its midcell localization in these *mreB*_{Q26P} cells (Fig. 2E), we conclude that MreB has no apparent positive or inhibitory effect on PBP2 accumulation at the FtsZ ring location.

Transition under environmental conditions causes the accumulation of PBP2 at the FtsZ ring location. Our observation of PBP2 recruitment to the FtsZ ring was inconsistent with previous reports (14, 15), raising the possibility that a difference in experimental conditions may be responsible for the discrepancy. We noted that in the previous studies, M2G cultures were used, whereas we used PYE cultures. Indeed, the midcell accumulation of GFP-PBP2 observed when using PYE cultures (Fig. 3A) was largely abrogated when cells were grown in M2G medium (Fig.

3B) instead of PYE medium, as evident from the relative uniformity of fluorescence seen in the demograph. In both cases, M2G agarose pads were used for visualization.

Since *C. crescentus* grows faster in the more nutrient-rich PYE medium, we examined whether PBP2 accumulation near midcell was dependent on the growth rate by varying the temperature. At 20 and 23°C, PYE cultures displayed doubling times of 235 ± 10 and 162 ± 4 min (mean \pm standard deviation [SD], $n = 3$ independent experiments), respectively, which are longer than the doubling time of M2G cultures at 30°C (115 ± 2 min, $n = 3$). Yet, GFP-PBP2 still accumulated near midcell when cells were pre-grown in liquid PYE culture medium at 20 or 23°C (see Fig. S3 in the supplemental material), indicating that it is not the growth rate but rather some aspect of the medium that affects PBP2 localization.

Surprisingly, the PYE culture medium *per se* did not cause the difference in PBP2 localization. Instead, it was the transition from

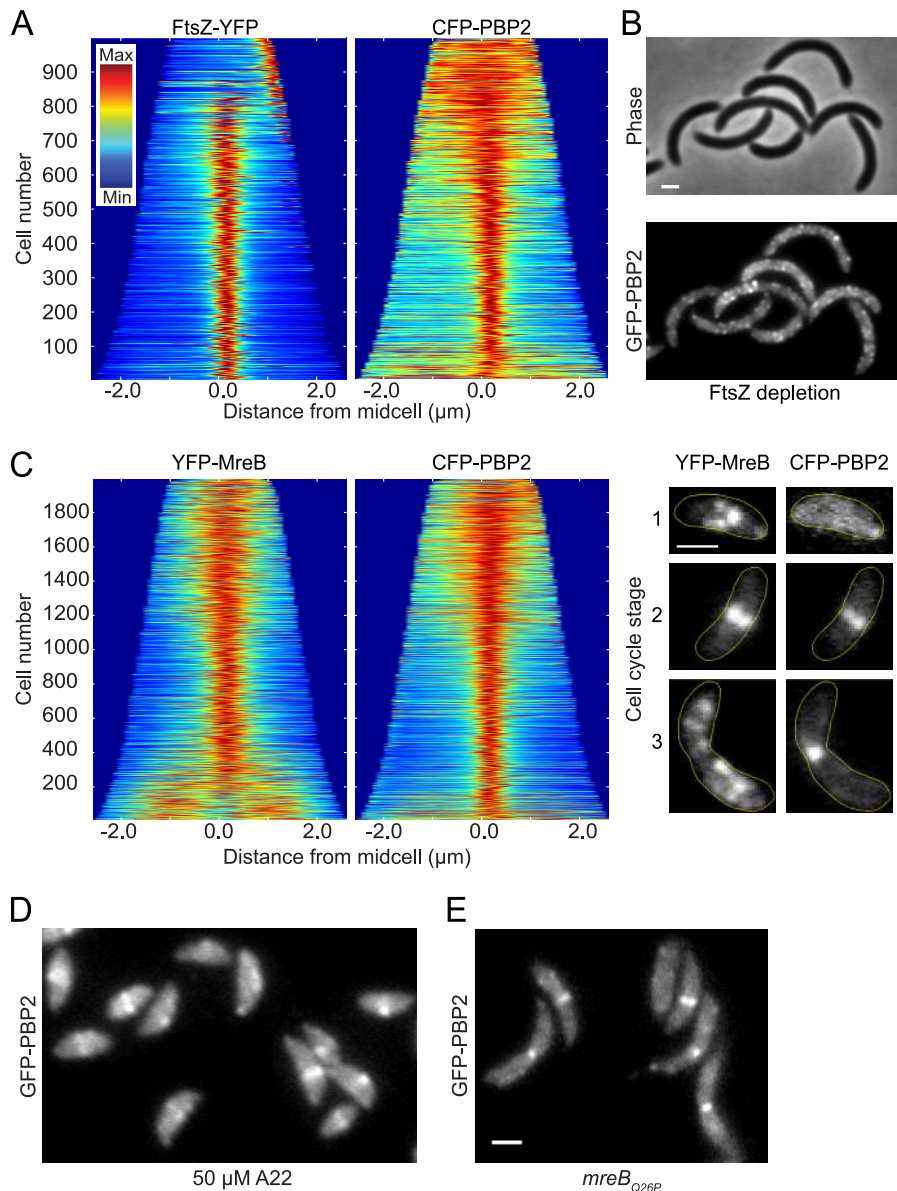


FIG 2 PBP2 colocalizes with MreB near midcell in an FtsZ-dependent but MreB-independent manner. (A) Demographs of CJW3402 cells producing FtsZ-YFP and CFP-PBP2. Cells were grown in PYE, and the synthesis of FtsZ-YFP and CFP-PBP2 was induced by adding xylose and vanillic acid for 4 h prior to imaging on an M2G pad. (B) Micrographs showing the localization of GFP-PBP2 in FtsZ-depleted cells. CJW3396 cells were grown in PYE containing vanillic acid, the inducer of *ftsZ* expression. Xylose, the inducer of *gfp-pbp2* expression, was added to the culture 2 h prior to cell synchronization. Swarmer cells were isolated and resuspended in PYE containing xylose but not vanillic acid. After 2 h of growth and FtsZ depletion, the cells were spotted and imaged on M2G pads. (C) Demographs and representative micrographs of cells (strain CJW3397) producing YFP-MreB and CFP-PBP2. Cells were first grown in PYE medium with xylose and vanillic acid for 4 h to induce the expression of YFP-MreB and CFP-PBP2, respectively, prior to microscopy on M2G agarose pads. (D) Fluorescent micrograph showing A22-treated cells producing GFP-PBP2 (strain CJW2135). Cells were grown in PYE medium containing xylose for 2 h to induce GFP-PBP2 synthesis followed by 2 h of A22 (50 μM) treatment before microscopy on M2G pads. (E) Micrograph showing the localization of GFP-PBP2 in CJW3403 cells carrying the *mreB*_{Q26P} mutation. Cells were grown in PYE, and synthesis of GFP-PBP2 was achieved by addition of xylose for 4 h prior to imaging on M2G pads. Bar, 1 μm.

the PYE culture to the M2G pad that caused midcell accumulation of PBP2, as spotting cells from a PYE culture to a PYE pad (i.e., an agarose pad containing PYE instead of M2G) for visualization did not result in midcell accumulation of mCherry-PBP2 (Fig. 3C). PBP2 localization was, on the other hand, insensitive to the transition from the M2G culture to the PYE pad (Fig. 3D). Midcell accumulation was observed not only when cells grown in PYE were visualized on an M2G pad (Fig. 3A) but also when cells

grown in PYE were washed in M2G and visualized in M2G liquid (instead of on an M2G agarose pad; data not shown).

Relocation of PBP2 to midcell happens fast upon medium change whereas the return of PBP2 to its patchy localization is slow and growth dependent. Our data so far indicated that a switch from PYE to M2G medium results in PBP2 relocation to the FtsZ ring location. The PBP2 relocation event is not controlled by changes in gene expression, as midcell localization of GFP-

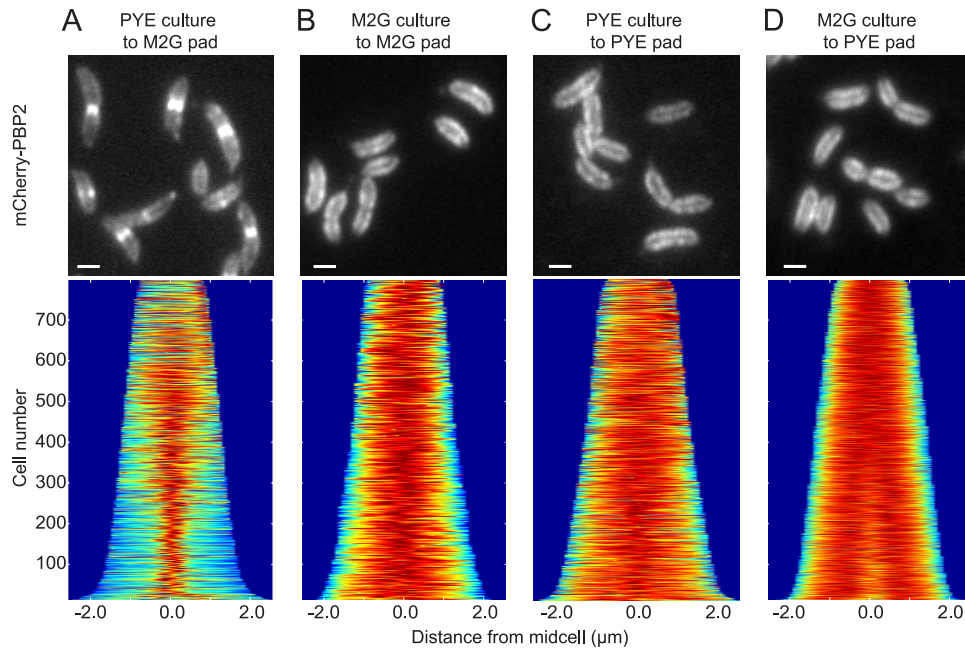


FIG 3 Relocation of PBP2 to the division site is dependent on changing the growth medium from PYE to M2G. Demographs and representative images of JAT878 cells producing mCherry-PBP2 after 3 h of induction with vanillic acid. (A) Cells from a PYE culture were imaged on an M2G pad. (B) Cells from an M2G culture were imaged on an M2G pad. (C) Cells from a PYE culture were imaged on a PYE pad. (D) Cells from an M2G culture were imaged on a PYE pad. Bars, 1 μm .

PBP2 still occurred when the cells were pretreated with the transcription inhibitor rifampin or the translation inhibitor chloramphenicol (see Fig. S4 in the supplemental material).

The relocation is remarkably quick, since it was already initiated within the 40 s that it took to spot cells from a PYE culture onto an M2G pad and image them on the microscope (Fig. 4A). The relocation process was complete within 2 min, as evident from tight midcell accumulation that remained unchanged over the following 3 min (Fig. 4A). Thus, relocation of mCherry-PBP2 to midcell is likely too fast to involve changes in peptidoglycan composition through remodeling. Even a transient exposure to M2G was sufficient to cause midcell relocation. This was shown by growing cells in PYE and then washing the cells in M2G prior to imaging them on a PYE agarose pad (Fig. 4B). In this assay, the cells were exposed to M2G medium for only approximately 3 min during the wash. No relocation to midcell was observed for PBP2 if the wash was a PYE solution (Fig. 4B) instead of M2G.

Next, we performed time-lapse experiments on cells that were grown on a PYE culture but imaged on an M2G pad and showed that PBP2 returns to a patchy localization over time (Fig. 4C). This redistribution was, however, slow and took approximately 2 h, which corresponds to about 1 to 2 generations. Surprisingly, the redistribution of mCherry-PBP2 appeared progressive, with the mCherry-PBP2 band at midcell getting wider and wider over time (Fig. 4C), as if PBP2 localization were expanding concomitantly with peptidoglycan growth (1). This redistribution required cell growth, as it was inhibited when cells were spotted on an M2 pad that lacked glucose (carbon source) for growth (Fig. 4D).

We concluded from these experiments that in response to a switch from PYE to M2G, PBP2 relocation to midcell is very rapid (≤ 40 s) but temporary because PBP2 gradually returns to a patchy localization; this return to patchy localization is, however, slow (~ 1 to 2 generations) and dependent on cell growth.

An upshift in medium osmolality is sufficient to cause PBP2 recruitment to midcell. Since PBP2 relocation to the FtsZ ring location occurs when the extracellular environment changes from PYE to M2G, we investigated what physical or chemical differences between these two media might cause PBP2 relocation. PYE and M2G media notably differ in chemical composition and pH. However, despite intensive efforts, we were unable to link PBP2 relocation to the presence of a specific chemical ingredient or to a difference in pH (data not shown). Interestingly, measurements with a vapor pressure osmometer revealed that PYE and M2G media also differ in osmolality (Fig. 5A). (Note that osmolality, which is the measure of osmoles of solute per kilogram of solvent, often is the preferred measure as it is insensitive to changes in pressure and temperature, unlike osmolarity, which is the measure of osmoles per liter of solution.) Perhaps counterintuitively, the osmolality of the nutrient-rich PYE medium (21.7 ± 1.5 mosmol/kg, mean \pm SD, $n = 3$ measurements) was lower than that of the minimal M2G medium (52.6 ± 1.2 mosmol/kg, $n = 3$) (Fig. 5A). While richer in nutrients because of the presence of yeast extract and peptone (0.1 and 0.2%, respectively), PYE has fewer osmolytes than does M2G, which contains M2 salts (6.1 mM Na_2HPO_4 , 3.9 mM KH_2PO_4 , and 5.6 mM NH_4Cl), 11.1 mM glucose, and other, less-abundant components (0.5 mM MgSO_4 , 0.5 mM CaCl_2 , and 0.01 mM FeSO_4).

Using a PYE culture/wash/PYE pad assay in which the only variable is the composition of the wash solution, we discovered that any solutions with an osmolality higher than that of PYE resulted in mCherry-PBP2 localization near midcell. For example, phosphate-buffered saline (PBS), which is commonly used as a wash solution in biological research, resulted in relocation of PBP2 to midcell (Fig. 5B), similarly to an M2G wash and unlike a PYE wash (Fig. 4B). The osmolality of PBS was 280 ± 2.6 mosmol/kg ($n = 3$), over 10-fold higher than that of PYE (Fig.

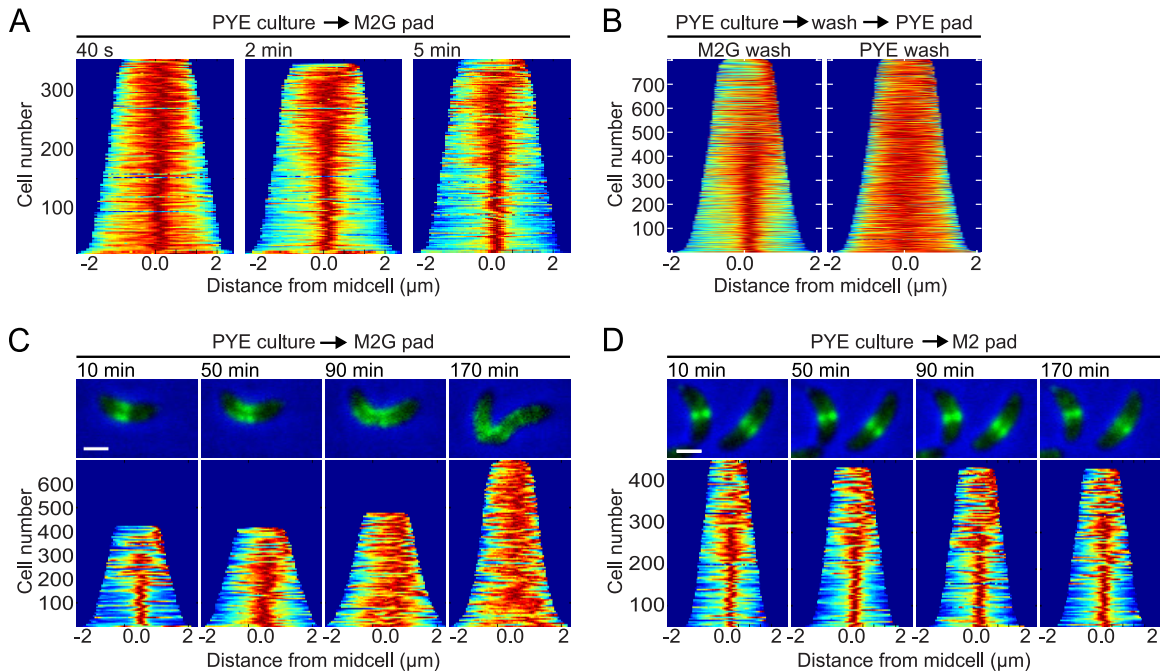


FIG 4 Relocation of PBP2 to midcell happens fast upon medium change whereas the return of PBP2 to its dispersed localization is slow and growth dependent. (A) Demographs showing mCherry-PBP2 localization at selected time points (40 s, 2 min, and 5 min) following an osmotic upshift. JAT878 cells producing mCherry-PBP2 (by induction with vanillic acid for 3 h) were grown in PYE and imaged on an M2G pad lacking vanillic acid. The first image was acquired 40 s after spotting cells on the pad. Additional images were taken every 20 s for up to 5 min. (B) Demographs showing mCherry-PBP2 localization following a brief wash in either M2G (osmotic upshift) or PYE (no osmotic shock). JAT878 cells producing mCherry-PBP2 (by induction with vanillic acid for 3 h) were grown in PYE and then washed in M2G or PYE medium before being spotted on a PYE pad. (C) Demographs showing mCherry-PBP2 localization at selected time points following an osmotic upshift. JAT878 cells producing mCherry-PBP2 (by induction with vanillic acid for 3 h) were grown in PYE and spotted on M2G for time-lapse imaging. (D) Same procedure as that in panel C except that cells were washed once with M2 (containing all the constituents of M2G except glucose) and spotted on an agarose pad containing M2.

5A). The type of components used to increase osmolality (inorganic or organic) did not seem to matter. For instance, brief exposure to $1\times$ M2 salts or PYE medium containing 20 mM NaCl or 2.5% sucrose (73 mM) all resulted in mCherry-PBP2 relocation to midcell (Fig. 5B). All of these solutions have higher osmolality than that of PYE (Fig. 5A). Conversely, purified water, which has a lower osmolality than that of PYE (Fig. 5A), had no effect on mCherry-PBP2 localization (Fig. 5B). We also noted small differences in PBP2 concentrations at the pole, but they tended to vary from experiment to experiment, suggesting that they may be caused by minute differences in procedures (e.g., in the hydration of the pad or in the time between washing and imaging). However, in all cases, an upshift in osmolality was reproducibly accompanied with a relocation of mCherry-PBP2 to the FtsZ ring location.

We obtained similar results when using an M2G culture/wash/M2G pad assay (instead of PYE culture/wash/PYE pad) in which we started with M2G cultures, washed them with solutions of various osmolalities, and imaged them on an M2G pad. Again, when the osmolality of the wash solutions was lower than or equal to that of M2G, such as with PYE, M2G, M2 salts, and purified H₂O (Fig. 5C), mCherry-PBP2 retained its dispersed patchy distribution. In contrast, wash solutions of higher osmolality than M2G, such as $3\times$ M2 salts or M2G medium containing 20 mM NaCl or 2.5% sucrose (Fig. 5A), caused mCherry-PBP2 relocation to midcell (Fig. 5C). Thus, whether cells are initially present in low (PYE)- or higher (M2G)-osmolality medium does not seem to matter; what seems important for PBP2 relocation to occur is an increase in external osmolality.

We also noted that the quality of the agarose pads used for microscopy can matter, as any significant drying increases the concentration of solutes in the pad, creating an osmotic upshift (data not shown).

C. crescentus displays low osmotolerance. We wondered if this osmotic response relates to the ecological niche of *C. crescentus*. *C. crescentus* is an oligotroph because of its ability to thrive in environments containing very low levels of nutrients, such as lakes and streams. These environments are also characterized by a very low osmolality. The rich (complex) medium of choice for *C. crescentus* growth in the laboratory is PYE, which is not only poorer in nutrients but also ~ 20 -fold lower in osmolality than LB (Fig. 6A). M2G is the most common minimal medium used by *Caulobacter* researchers; it has the same amount of carbon as does the minimal medium M9 glucose commonly used for *E. coli* but has an osmolality ~ 5 -fold lower than that of M9 glucose (Fig. 6A), primarily because of a much lower concentration of phosphate buffer (3.98 mM versus 25 mM). We found that *C. crescentus* is unable to grow in LB or M9 glucose after overnight culture (data not shown).

Increasing the osmolality of M2G by adding increasing concentrations of NaCl (from 10 mM to 80 mM) gradually decreased the growth of *C. crescentus* as shown by the increase in doubling time (Fig. 6B). Growth was completely inhibited in M2G containing NaCl at concentrations of 85 mM or more (data not shown). *C. crescentus* was, however, able to grow in the presence of higher concentrations of NaCl when the osmolality of the medium was decreased to compensate. For example, exponential growth was observed in the presence of up to

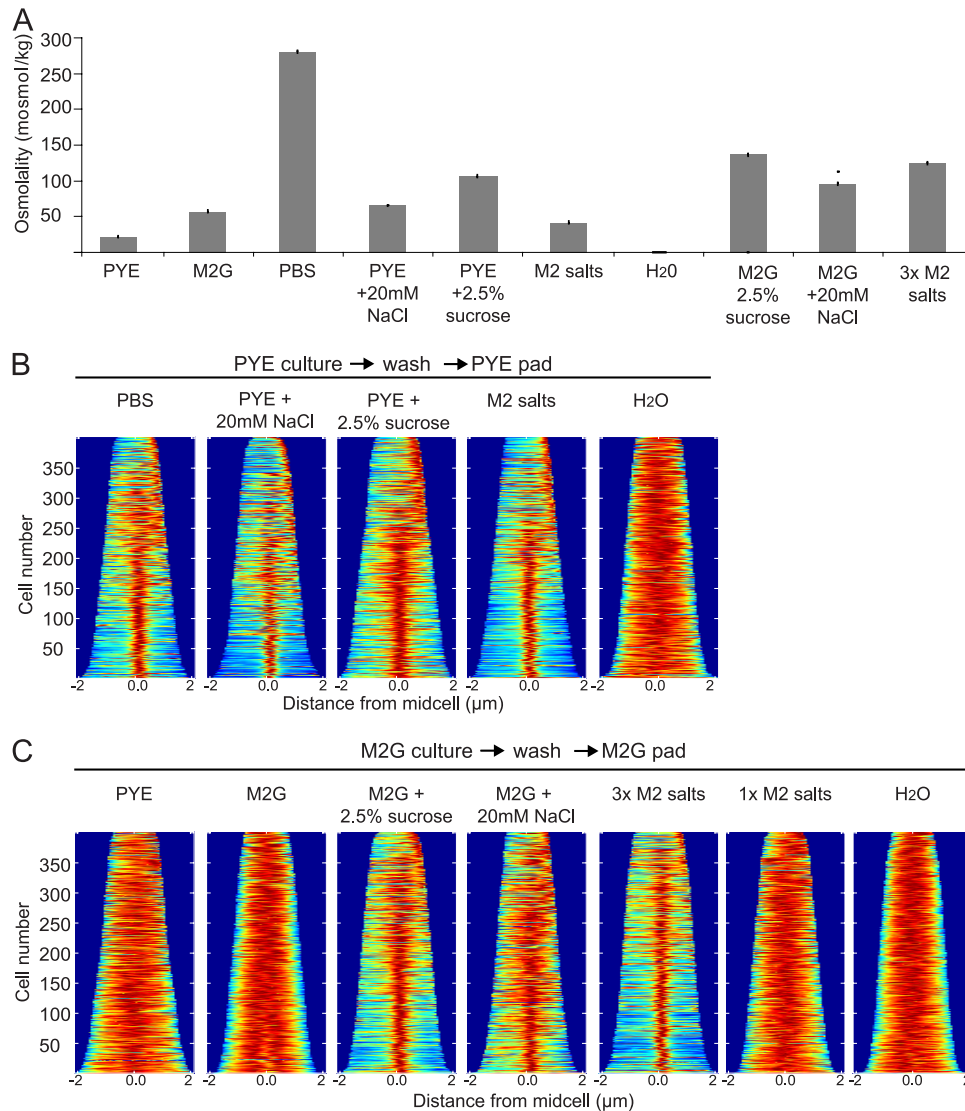


FIG 5 An upshift in medium osmolality is sufficient to cause PBP2 recruitment to the FtsZ ring location. (A) The graph shows average osmolality measurements of indicated solutions obtained from 3 independent measurements. Error bars indicate the standard deviations of measurement. (B) Demographs showing mCherry-PBP2 localization from PYE cultures of JAT878 cells that have been briefly washed in solutions of different osmolalities prior to imaging on PYE pads. mCherry-PBP2 synthesis was achieved by addition of vanillic acid for 3 to 4 h in the PYE cultures. (C) Same procedure as that in panel B except that M2G cultures and M2G pads were used.

95 mM NaCl when the concentrations of glucose, phosphate buffer, and nitrate in M2G were decreased by half (referred to as “M2G_{half}”; Fig. 6B). The trade-off was that these cultures reached stationary phase sooner (data not shown), as these osmolytes, which also are nutrients, become more rapidly depleted from the medium. Exponential growth was also faster in M2G_{half} than in M2G for the tested NaCl concentrations of 40 mM and above, as shown by a decrease in doubling time (Fig. 6B, top). For example, cells growing in M2G_{half} plus 60 mM NaCl had a doubling time of 141.8 ± 1.5 min (mean \pm SD, $n = 3$ biological replicates) compared to 197.2 ± 6.4 min ($n = 3$) for cells growing in M2G plus 60 mM NaCl. When the doubling times for the cultures grown in M2G or M2G_{half} containing various concentrations of NaCl were plotted as a function of osmolality (Fig. 6B, bottom) instead of NaCl concentrations

(Fig. 6B, top), the two curves overlapped, indicating that the growth inhibition is due to the increased external osmolality, rather than salt intolerance.

These observations suggest that in minimal medium (which lacks osmoprotectants), *C. crescentus* has a low osmotolerance with an upper limit of approximately 225 mosmol/kg (Fig. 6B). In contrast, *E. coli* grows in media with osmolalities as high as 3,000 mosmol/kg (25), which is consistent with its broad ecology (ranging from streams to the human gut).

The localization of *E. coli* PBP2 is largely unaffected by osmotic upshifts. We wondered whether the relocation of PBP2 in response to osmotic upshifts was somehow connected to the ecological niches of *C. crescentus*. If true, we expected bacteria such as *E. coli* to display no or little response. In *E. coli*, PBP2 has been reported to adopt a patchy localization throughout the cell mem-

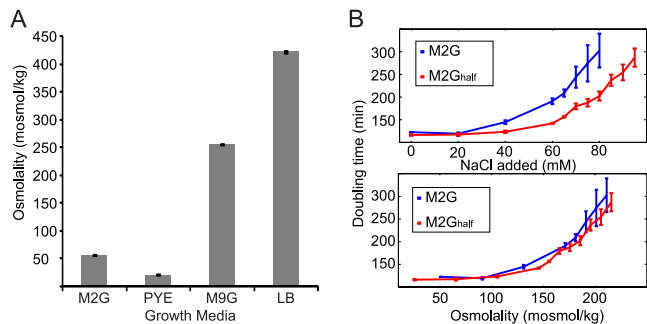


FIG 6 *C. crescentus* growth is very sensitive to external osmolality. (A) The graph shows average osmolality measurements of indicated solutions obtained from 3 independent measurements. Error bars indicate the standard deviations of measurement. (B) Wild-type CB15N cells were grown in 3 replicates in either M2G or M2G_{half} (which consists of half the concentrations of glucose, phosphate buffer, and nitrate found in M2G) supplemented with 0, 20, 40, 60, 65, 70, 75, 80, 85, 90, 95, or 100 mM NaCl. Growth was monitored using a microplate reader, and doubling times in the exponential phase of the cultures were plotted as a function of NaCl concentration (top) or osmolality of the growth medium (bottom). The plots show mean values \pm SDs.

brane with some ring-like accumulations in the midcell region (11, 35). We observed a similar localization pattern for a GFP-PBP2 fusion in *E. coli* cells grown in LB or M9G medium, as shown in demographs (Fig. 7A and B), and this pattern was maintained following an osmotic upshift with the addition of 100 mM NaCl.

Even when the cells were grown in low-osmolality PYE medium and spotted on PYE pads containing increasing concentrations of NaCl (20 to 60 mM), there were no significant differences in the GFP-PBP2 localization profile (Fig. 7C). Under these conditions, PBP2 relocates to the division site in *C. crescentus*. These results support the notion that the sensitivity of PBP2 to osmotic stress might reflect ecological differences between *C. crescentus* and *E. coli*.

The localization of PBP1a and RodA is also affected by osmotic upshifts in *C. crescentus*. There are a large number of proteins involved in the biosynthesis and regulation of the cell wall in *C. crescentus*. Some of them, such as the morphogenetic protein MreB (19, 20), the precursor PG synthesis enzyme MurG (1), and the morphogenetic protein RodZ (3), have been shown to localize to the FtsZ ring. We found that these midcell accumulations occurred whether or not the cells were subjected to an osmotic upshift (see Fig. S5 in the supplemental material). We also examined the localization of MreC, which has been reported to have a patchy localization near the cell membrane in *C. crescentus* (14). This pattern remained dispersed and patchy even when the cells experienced an osmotic upshift (see Fig. S5).

We did, however, observe a difference in localization pattern for fluorescent fusions of RodA and PBP1a in response to an osmotic upshift (Fig. 8A and B), although not to the same extent as with PBP2. RodA, a polytopic membrane protein of the SEDS

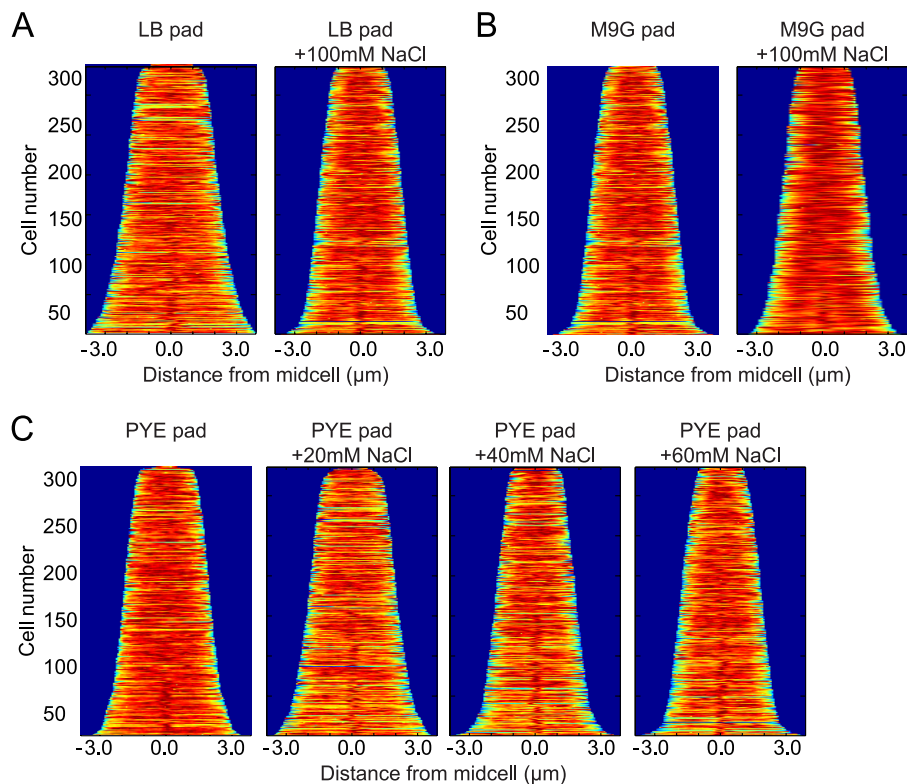


FIG 7 The localization of *E. coli* PBP2 is largely unaffected by osmotic upshifts. Demographs showing GFP-PBP2 localization under different growth conditions. In all cases, *E. coli* cells (strain LMC1840) were grown at 30°C and induction of GFP-PBP2 synthesis was achieved by addition of IPTG for 40 min. (A) Cells were grown in LB medium and imaged on pads containing either LB or LB plus 100 mM NaCl. (B) Cells were grown in M9G medium and imaged on pads containing either M9G or M9G plus 100 mM NaCl. (C) Cells were grown in PYE medium and imaged on pads containing either PYE or PYE supplemented with the indicated concentration of NaCl.

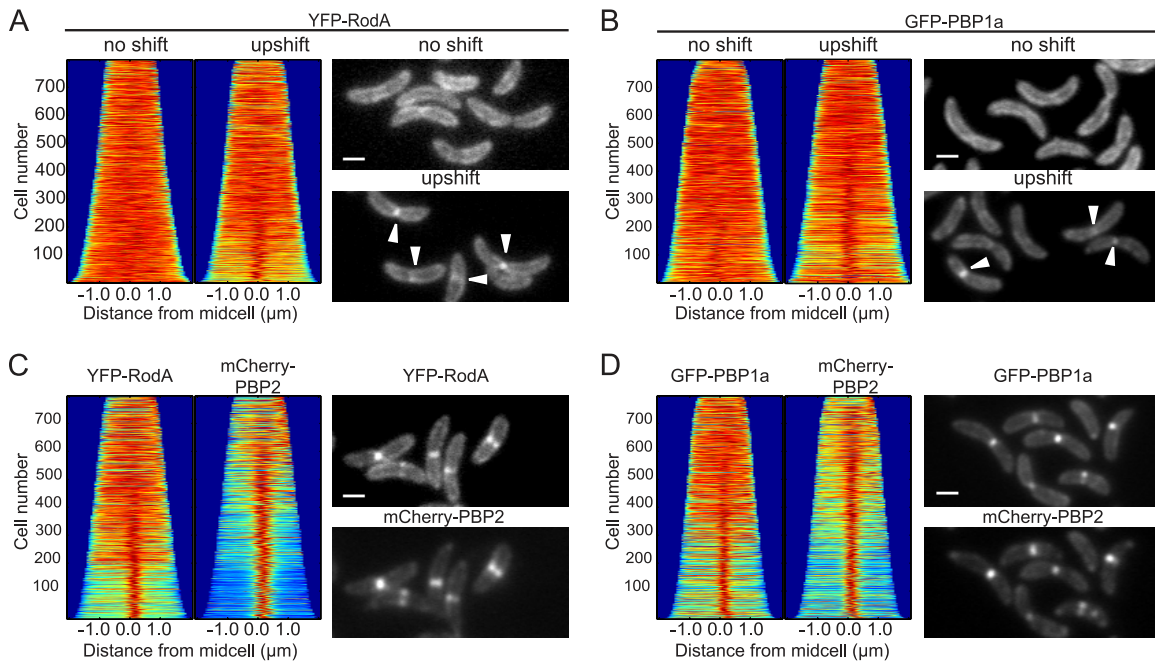


FIG 8 The localizations of PBP1a and RodA are also affected by osmotic upshifts in *C. crescentus*. (A) Demographs and representative images showing YFP-RodA localization in *C. crescentus* cells (strain CJW3207) grown in PYE medium and imaged on pads containing either M2G (no shift) or PYE (upshift). YFP-RodA synthesis was achieved by addition of xylose for 3 h before spotting cells on an agarose pad. Arrowheads indicate accumulation of YFP-RodA near midcell. Bars, 1 μm . (B) Same procedure as that in panel A except that CJW3288 cells producing GFP-PBP1a were imaged. Synthesis of GFP-PBP1a was induced with xylose 3 h prior to imaging. (C) Demographs and representative images showing the localization of YFP-RodA and mCherry-PBP2. CJW4621 cells were grown in PYE with xylose and vanillic acid for 3 h to induce the synthesis of both YFP-RodA and mCherry-PBP2 prior to imaging on an M2G pad. Bars, 1 μm . (D) Same procedure as that in panel C except that CJW4620 cells producing GFP-PBP1a and mCherry-PBP2 were imaged following induction of their synthesis with xylose and vanillic acid for 3 h.

family of PG precursor flippases, has been proposed to act in concert with PBP2 in PG synthesis during the elongation of *E. coli* (23, 30). Since RodA localization has not been reported in *C. crescentus*, we created a strain (CJW3207) in which a YFP-RodA fusion is produced under the xylose-inducible promoter from the chromosome. When cells were grown in PYE liquid medium and spotted on an M2G pad (resulting in an osmotic upshift), YFP-RodA displayed dispersed/patchy membrane localization in nondividing cells and a weak but discernible midcell accumulation that was most apparent in deeply constricted cells (Fig. 8A). Such accumulation was less prevalent in cells grown in M2G medium and spotted onto an M2G pad (i.e., no osmotic shift) (Fig. 8A), suggesting a response to an increase in external osmolality.

Similarly, a GFP fusion to a PBP1a homolog (CC1516), which contains transglycosylase and transpeptidase domains, displayed a discernible accumulation at the site of division in many constricted cells following osmotic upshift; such midcell accumulation was much less apparent without osmotic upshift (Fig. 8B).

Since RodA and PBP1a have been proposed to be part of a multienzyme complex with PBP2 (for a recent review, see reference 32), we considered the possibility that the midcell accumulation of YFP-RodA and GFP-PBP1a under osmotic-upshift conditions might be weak because the higher level of these xylose-inducible fusions results in saturation of the natively expressed PBP2 at midcell. If true, we would expect that a concomitant overproduction of PBP2 would result in a more prominent midcell accumulation of YFP-RodA and GFP-PBP1a under osmotic-upshift conditions. This was indeed what we observed. When

mCherry-PBP2 and YFP-RodA were coexpressed from the vanillic acid- and xylose-inducible promoters, respectively, the midcell accumulation of YFP-RodA was considerably enhanced following the hyperosmotic shock (Fig. 8C). The same happened for GFP-PBP1a (Fig. 8D).

DISCUSSION

In nature, bacterial species are found in vastly different osmotic environments. While some species display broad osmotolerance, many, if not most, do not, and yet they remain susceptible to osmotic fluctuations within their habitats. In this study, we show that *C. crescentus* displays a narrow dynamic range of osmotolerance, with an upper limit of growth osmolality of about 225 mosmol/kg (in a minimal medium lacking osmoprotectants). This is consistent with the ecological distribution of this organism in the wild.

We also show that in *C. crescentus*, PBP2 and at least two other cell wall proteins, RodA and PBP1a, are recruited to the divisome following osmotic upshifts. This effect occurs even in response to an increase in external osmolality as low as 40 mosmol/kg (for example, by adding ~ 20 mM NaCl to the growth medium, which corresponds to an addition of only 1.2 g of NaCl per liter of solution). This result has important implications, as many laboratory procedures routinely include steps in which cells are exposed to an environment with a different osmolality (e.g., washing in buffered solutions). Osmotic upshifts as low as 40 mosmol/kg are also likely to occur in natural environments, which often are unstable. Furthermore, many bacteria, including *Caulobacter* species, can form

high-cell-density biofilms where the osmolality is expected to fluctuate, for example, with the release of cellular components from cell death occurring within the biofilm.

While very small in absolute terms, an osmotic upshift of 40 mosmol/kg is considerable in relative terms when it occurs in low-osmolality environments. For instance, the PYE medium has an osmolality of ~22 mosmol. An increase in 40 mosmol generates an approximately 3-fold increase in the osmolality of the growth medium. Such a relative increase causes water to flow out of the cytoplasm. Cells respond to an increase in external osmolality by transporting and synthesizing compatible solutes to increase their internal osmotic strength and return water to the cytoplasm (8, 38). Long-term adaptation in bacteria, including *C. crescentus* (2, 41), involves gene expression and cellular remodeling.

Efflux of water due to an osmotic upshift results in loss of turgor pressure and shrinkage of the cytoplasmic space (6). Concomitantly, the PG becomes less stretched. The relocation of PBP2 to the division site does not require gene expression, and the observation that it occurs remarkably fast (≤ 40 s) suggests that this event happens in response to the initial phase of osmotic stress. The specific event triggering PBP2 relocation is unclear. Perhaps PBP2 senses the relaxation of the PG layer or local contractions of the cytoplasmic membrane, which may affect the interaction of the inner-membrane-anchored PBP2 with its PG substrate. It is possible that the division plane is less sensitive to such perturbations because of the accumulation of trans-envelope complexes (e.g., the divisome and the essential Tol/Pal complex [39]) that connect the outer membrane, the PG, and the inner membrane.

Interestingly, after osmotic upshift, dispersion of PBP2 from midcell is very slow and requires cell growth. The observation that PBP2 is recruited to the divisome for one to two generations raises the possibility that PBP2 may participate in the adaptation to higher-osmolality environments. It is theoretically possible that the accumulation of PBP2 at the FtsZ ring location may increase the cross-linking of the septal PG and thereby help strengthen the septal PG during the recovery period when the cell remains vulnerable. Addressing these hypotheses will require a better understanding of cell wall morphogenesis and osmotic stress.

While a role for PBP2 in osmotic adaptation in *C. crescentus* remains speculative, our study clearly uncovers a previously unsuspected link between important cell wall proteins (PBP2, RodA, and PBP1a) and osmotic stress in *C. crescentus*. PBP2 and RodA are often referred to as cell elongation-specific proteins essential for lateral PG growth. Our study shows that in *C. crescentus*, these proteins can be recruited to the divisome upon osmotic upshifts. Under these conditions, PBP3 remains colocalized with the FtsZ ring (data not shown), indicating that both PBP2 and PBP3 transpeptidases coexist at the division plane. This suggests that the notions of phase specificity (cell elongation for PBP2 and cell division for PBP3) and mutual exclusivity of these transpeptidases are likely oversimplifications, a view also supported by studies in other bacteria (11, 28, 35). Do PBP2 and PBP3 use different PG substrates near midcell, or do they compete for the same substrates? Are these two essential transpeptidases part of the same PG-synthesizing complexes? *C. crescentus* can offer a valuable model system for addressing these questions in the future.

In conclusion, our findings uncover an unsuspected environmental regulation of the localization of proteins involved in cell wall morphogenesis and stress the need for a better understanding

of the fluctuating physicochemical environments in which bacterial cells live.

ACKNOWLEDGMENTS

We thank Tanneke Den Blaauwen for the LMC1840 strain and Janet Wood and the members of the Jacobs-Wagner laboratory for helpful discussion. We are also grateful to Michael Higley for sharing his osmometer.

This work was supported by the National Institutes of Health (GM076698 and GM065835 to C.J.-W.). C.J.-W. is an Investigator of the Howard Hughes Medical Institute. R.P. was supported in part by a Yale Anderson fellowship. C.N.T. was in part supported by a Yale College Dean's Office Science, Technology and Research Scholars (STARS II) fellowship. T.C. was in part supported by a Yale Anderson fellowship and by a postdoctoral fellowship (SFRH/BPD/26232/2006) from the Fundação para a Ciência e Tecnologia.

REFERENCES

- Aaron M, et al. 2007. The tubulin homologue FtsZ contributes to cell elongation by guiding cell wall precursor synthesis in *Caulobacter crescentus*. *Mol. Microbiol.* 64:938–952.
- Alvarez-Martinez CE, Lourenco RF, Baldini RL, Laub MT, Gomes SL. 2007. The ECF sigma factor sigma(T) is involved in osmotic and oxidative stress responses in *Caulobacter crescentus*. *Mol. Microbiol.* 66:1240–1255.
- Alyahya SA, et al. 2009. RodZ, a component of the bacterial core morphogenic apparatus. *Proc. Natl. Acad. Sci. U. S. A.* 106:1239–1244.
- Bean GJ, et al. 2009. A22 disrupts the bacterial actin cytoskeleton by directly binding and inducing a low-affinity state in MreB. *Biochemistry* 48:4852–4857.
- Cabeen MT, Jacobs-Wagner C. 2010. The bacterial cytoskeleton. *Annu. Rev. Genet.* 44:365–392.
- Cayley DS, Guttman HJ, Record MT, Jr. 2000. Biophysical characterization of changes in amounts and activity of *Escherichia coli* cell and compartment water and turgor pressure in response to osmotic stress. *Biophys. J.* 78:1748–1764.
- Costa T, Priyadarshini R, Jacobs-Wagner C. 2008. Localization of PBP3 in *Caulobacter crescentus* is highly dynamic and largely relies on its functional transpeptidase domain. *Mol. Microbiol.* 70:634–651.
- Csonka LN. 1989. Physiological and genetic responses of bacteria to osmotic stress. *Microbiol. Rev.* 53:121–147.
- Daniel RA, Errington J. 2003. Control of cell morphogenesis in bacteria: two distinct ways to make a rod-shaped cell. *Cell* 113:767–776.
- Daniel RA, Harry EJ, Errington J. 2000. Role of penicillin-binding protein PBP 2B in assembly and functioning of the division machinery of *Bacillus subtilis*. *Mol. Microbiol.* 35:299–311.
- Den Blaauwen T, Aarsman ME, Vischer NO, Nanninga N. 2003. Penicillin-binding protein PBP2 of *Escherichia coli* localizes preferentially in the lateral wall and at mid-cell in comparison with the old cell pole. *Mol. Microbiol.* 47:539–547.
- Den Blaauwen T, Pas E, Edelman A, Spratt BG, Nanninga N. 1990. Mapping of conformational epitopes of monoclonal antibodies against *Escherichia coli* penicillin-binding protein 1B (PBP 1B) by means of hybrid protein analysis: implications for the tertiary structure of PBP 1B. *J. Bacteriol.* 172:7284–7288.
- de Pedro MA, Quintela JC, Holtje JV, Schwarz H. 1997. Murein segregation in *Escherichia coli*. *J. Bacteriol.* 179:2823–2834.
- Divakaruni AV, Loo RR, Xie Y, Loo JA, Gober JW. 2005. The cell-shape protein MreC interacts with extracytoplasmic proteins including cell wall assembly complexes in *Caulobacter crescentus*. *Proc. Natl. Acad. Sci. U. S. A.* 102:18602–18607.
- Dye NA, Pincus Z, Theriot JA, Shapiro L, Gitai Z. 2005. Two independent spiral structures control cell shape in *Caulobacter*. *Proc. Natl. Acad. Sci. U. S. A.* 102:18608–18613.
- El Ghachi M, et al. 2011. Characterization of the elongosome core PBP2: MreC complex of *Helicobacter pylori*. *Mol. Microbiol.* 82:68–86.
- Ely B. 1991. Genetics of *Caulobacter crescentus*. *Methods Enzymol.* 204:372–384.
- Evinger M, Agabian N. 1977. Envelope-associated nucleoid from *Caulobacter crescentus* stalked and swarmer cells. *J. Bacteriol.* 132:294–301.
- Figge RM, Divakaruni AV, Gober JW. 2004. MreB, the cell shape-determining bacterial actin homologue, co-ordinates cell wall morphogenesis in *Caulobacter crescentus*. *Mol. Microbiol.* 51:1321–1332.

20. Gitai Z, Dye N, Shapiro L. 2004. An actin-like gene can determine cell polarity in bacteria. *Proc. Natl. Acad. Sci. U. S. A.* **101**:8643–8648.
21. Gitai Z, Dye NA, Reisenauer A, Wachi M, Shapiro L. 2005. MreB actin-mediated segregation of a specific region of a bacterial chromosome. *Cell* **120**:329–341.
22. Holtje JV. 1998. Growth of the stress-bearing and shape-maintaining murein sacculus of *Escherichia coli*. *Microbiol. Mol. Biol. Rev.* **62**:181–203.
23. Ishino F, et al. 1986. Peptidoglycan synthetic activities in membranes of *Escherichia coli* caused by overproduction of penicillin-binding protein 2 and rodA protein. *J. Biol. Chem.* **261**:7024–7031.
24. Paradis-Bleau C, et al. 2010. Lipoprotein cofactors located in the outer membrane activate bacterial cell wall polymerases. *Cell* **143**:1110–1120.
25. Record MT, Jr, Courtenay ES, Cayley S, Guttman HJ. 1998. Biophysical compensation mechanisms buffering *E. coli* protein-nucleic acid interactions against changing environments. *Trends Biochem. Sci.* **23**:190–194.
26. Simon R, Priefer U, Puhler A. 1983. A broad host range mobilization system for *in vivo* genetic engineering: transposon mutagenesis in gram negative bacteria. *Biotechnology* **1**:784–790.
27. Sliusarenko O, Heinritz J, Emonet T, Jacobs-Wagner C. 2011. High-throughput, subpixel precision analysis of bacterial morphogenesis and intracellular spatio-temporal dynamics. *Mol. Microbiol.* **80**:612–627.
28. Slovak PM, Porter SL, Armitage JP. 2006. Differential localization of Mre proteins with PBP2 in *Rhodobacter sphaeroides*. *J. Bacteriol.* **188**:1691–1700.
29. Spratt BG. 1975. Distinct penicillin binding proteins involved in the division, elongation, and shape of *Escherichia coli* K12. *Proc. Natl. Acad. Sci. U. S. A.* **72**:2999–3003.
30. Tamaki S, Matsuzawa H, Matsuhashi M. 1980. Cluster of mrdA and mrdB genes responsible for the rod shape and mecillinam sensitivity of *Escherichia coli*. *J. Bacteriol.* **141**:52–57.
31. Thanbichler M, Iniesta AA, Shapiro L. 2007. A comprehensive set of plasmids for vanillate- and xylose-inducible gene expression in *Caulobacter crescentus*. *Nucleic Acids Res.* **35**:e137. doi:10.1093/nar/gkm818.
32. Typas A, Banzhaf M, Gross CA, Vollmer W. 2011. From the regulation of peptidoglycan synthesis to bacterial growth and morphology. *Nat. Rev. Microbiol.* **10**:123–136.
33. Typas A, et al. 2010. Regulation of peptidoglycan synthesis by outer-membrane proteins. *Cell* **143**:1097–1109.
34. Varma A, de Pedro MA, Young KD. 2007. FtsZ directs a second mode of peptidoglycan synthesis in *Escherichia coli*. *J. Bacteriol.* **189**:5692–5704.
35. Vats P, Shih YL, Rothfield L. 2009. Assembly of the MreB-associated cytoskeletal ring of *Escherichia coli*. *Mol. Microbiol.* **72**:170–182.
36. Vollmer W, Bertsche U. 2008. Murein (peptidoglycan) structure, architecture and biosynthesis in *Escherichia coli*. *Biochim. Biophys. Acta* **1778**:1714–1734.
37. Weiss DS, et al. 1997. Localization of the *Escherichia coli* cell division protein FtsI (PBP3) to the division site and cell pole. *Mol. Microbiol.* **25**:671–681.
38. Wood JM. 2007. Bacterial osmosensing transporters. *Methods Enzymol.* **428**:77–107.
39. Yeh YC, Comolli LR, Downing KH, Shapiro L, McAdams HH. 2010. The *Caulobacter* Tol-Pal complex is essential for outer membrane integrity and the positioning of a polar localization factor. *J. Bacteriol.* **192**:4847–4858.
40. Young KD. 2010. Bacterial shape: two-dimensional questions and possibilities. *Annu. Rev. Microbiol.* **64**:223–240.
41. Zuleta LF, Italiani VC, Marques MV. 2003. Isolation and characterization of NaCl-sensitive mutants of *Caulobacter crescentus*. *Appl. Environ. Microbiol.* **69**:3029–3035.